RSC Advances

ROYAL SOCIETY OF CHEMISTRY

www.rsc.org/advances

Graphical abstract

Both the physical and physiochemical properties of domestic and wild silkworm silk fibroin were studied, including surface energy and surface energy heterogeneity.

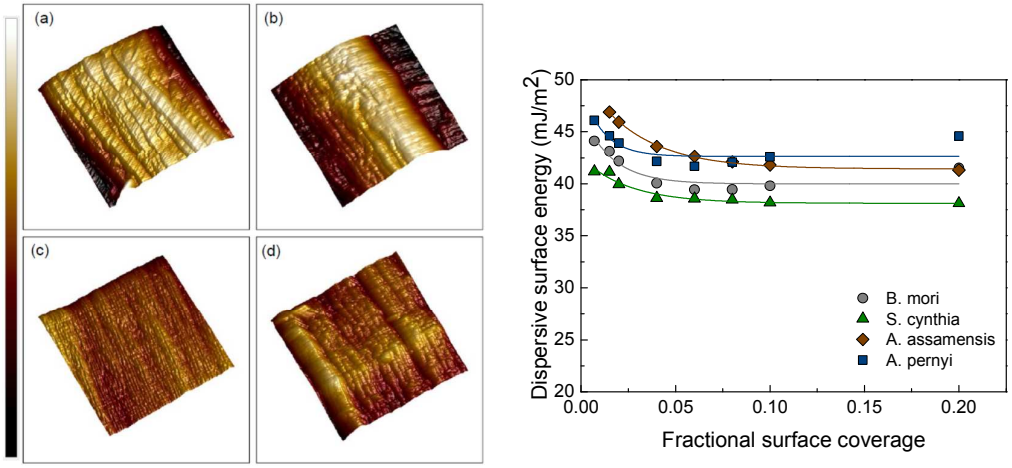

RSC Advances

RSCPublishing

ARTICLE

Surface Energy of Silk Fibroin and Mechanical Properties of Silk Cocoon Composites

Cite this: DOI: 10.1039/x0xx00000x

J. Zhang[a], S. Du[a], A. Kafi[a], B. Fox[a], J. L. Li[a], X.Y. Liu[b], R. Rajkhowa[a], X.G. Wang[a,c]

Received ooth January 2012,
Accepted ooth January 2012

DOI: 10.1039/x0xx00000x

www.rsc.org/

Silkworm cocoons are biological composite structures protecting the silkworms against environmental damage and physical attack by natural predators. In particular, some outdoor reared silk cocoons exhibit outstanding mechanical properties that are relevant to the higher level protection required to enhance the survival chance of silkworms while supporting their metabolic activity. The performance of composite materials strongly depends on the adhesion between the fibre reinforcement and matrix, with the surface properties of the fibres playing a key role in determining the level of adhesion achieved. For this reason it is important to study the surface properties of silk fibroin to further understand the composite properties of the cocoons. In this work, both the mechanical properties of the silk cocoons and silk fibroin were studied. The surface topography was examined using scanning probe microscopy (SPM), which revealed distinct longitudinal ridges and striations along the fibre axis of the four silk fibre types. The fibres were found to exhibit heterogeneity in surface energy as evidenced from inverse gas chromatography (IGC) measurements. The combination of excellent mechanical properties and the more energetically heterogeneous surface nature of the wild *A. pernyi* silk fibroin fibres correlates well with the excellent mechanical properties of the *A. pernyi* cocoons.

1. Introduction

Silkworm silk fibres are outstanding natural materials that have long been used for textiles. [1, 2] Silk-based materials have recently found applications in a growing number of areas including biodegradable medical scaffolds, implantable functional devices and tissue engineering products. [3, 4] While the properties of *Bombyx mori* (*B. mori*) cocoon silk and the major ampullate silks from a range of spiders have been extensively studied, [5-7] there are substantial knowledge gaps in understanding other silkworm silks including semi-domestic and wild silks and their cocoon structures. In nature, very thin and lightweight wild silkworm cocoons can protect silkworms from physical attacks from predators or environment while supporting their metabolic activity. [8, 9] It is known that the wild silkworm silks such as Chinese tussah silkworm *Antheraea pernyi* (*A. pernyi*) and semi-domestic *Antheraea assamensis* (*A. assamensis*) silks are remarkably similar to the Golden Orb Web spider (*Nephila Clavipes*) silk and they have the excellent balance of strength, extensibility and toughness, presumably due to similar protein structure. [10] Therefore the understanding of the mechanical property of such silkworm silks and their protective cocoon structure may provide insightful guidance for future bio-mimetic design of protective fibres and fibrous structures such as fabrics and textile composites.

A cocoon is a multilayer porous composite structure formed by continuous twin silk filaments (bave) bonded by silk gum (sericin). The compact cocoon structure is formed when a silkworm, along with spinning, wraps the twin silk filaments around its body through a gyrating motion of its head and cyclically bending and stretching of its body with different shapes in a programmed manner. [11, 12] The mechanical performance of composites depends on the properties of individual component as well as on the interfacial compatibility between the constituting materials. The performance of composites strongly depends on the strength of the fibre/matrix interfacial zone, which controls the stress transfer process between the reinforcement and the matrix. However, it is difficult to evaluate the interface when the boundary between fibre and matrix is not clear. Composite interfaces can be characterized by analysing the surfaces of the fibres before they are impregnated with matrix. [13] In the case of natural silk filaments, the interfacial properties can be examined through analysing the surface of the degummed fibres. Because the fibre/matrix interfacial region is closely related to the surface properties (e.g., surface energy, acid-base interactions, etc.) of both the fibres and matrix, characterisation of the surface properties would be necessary to understand the adhesion, including the topography study and the IGC tests of degummed silk fibres for this work. Despite of the importance of surface energy parameters in preparation and properties in silk/polymer composites, the surface characteristics of silkworm silks are scarcely reported in literature.

Our previous work on interlaminar peel tests has shown that the wild silkworm cocoons are uniquely tough composite structures; the maximum work-of-fracture of the wild cocoons (*A. pernyi* and *Antheraea mylitta, i.e. A. mylitta*) was approximately 1000 J/m^2, which was almost 10 times the value for the domesticated cocoon (*B.*

mori) and 3~4 times the value for the semi-domesticated cocoon (*A. assamensis*). [14, 15] For some applications, natural fibres offer advantages over conventional synthetic fibres such as carbon and glass fibres as the reinforcement for composites, i.e. low cost, renewability, acceptable specific strength properties and biodegradability. [16, 17] As one of the animal-based fibres, silk has received far less attention than plant-based fibres such as flax, jute, kenaf for the use as reinforcement in biocomposites. [18, 19] As a result, further study of various silkworm silks and more particularly wild silkworm silks and their naturally built composite structures, i.e. cocoons, have important practical implications for the development of new biodegradable and renewable composite materials.

This work employs a range of techniques to characterise both the physical and chemical properties, including surface energy and surface energy heterogeneity, of both domestic and wild silkworm silk fibroin. In particular, inverse gas chromatography (IGC) was used in the present study to characterize the surface properties (surface area, surface energy, heterogeneity and acid–base properties) of several silk fibres.

2. Materials and Methods

2.1 Materials

B. mori and *A. assamensis* silkworm cocoons were purchased from silk rearing houses in Northeast India; *A. mylitta* cocoons were collected from Central India and *A. pernyi* cocoons were collected from Northeast China. They were received as stifled cocoons, as commonly used prior to reeling silk filament for textile applications. The silk samples were degummed by washing the fibres for 30 min in a 1 wt% solution of Marseille soap and 0.5 wt% of Na_2CO_3 in boiling deionized water, followed by rinsing with deionized water. The process was repeated with fresh solutions twice for the *B. mori* and the *Samia cynthia (S. Cynthia)* cocoons and three times for the *A. pernyi* and the *A. assamensis* cocoons. The degummed silk fibres were then air dried. During silk sampling, the temperature was held constant at the ambient room temperature of 22 °C and the humidity was kept at 50–55%.

2.2 Physical Characterisation

2.2.1. Mechanical Testing

An Instron MicroTester (Model 5848; force resolution, 0.5% of the indicated load; position resolution 0.02 μ m) equipped with a 0.5 N load cell was used to measure the tensile properties of the silk fibroin. A gauge length of 20 mm with a measured error of 0.1 mm was used. The fibre was stretched until it broke and the strain rate was 50% per minute. The experiments were operated at 22ºC and the relative humidity was kept at 50~55%. 40 samples were tested for each silkworm silk type. The tensile properties of the cocoon walls were tested on an Instron 30K universal tester with a loading rate of 2 mm/min. The gauge length used was 10 mm and the cocoon wall samples were 5 mm wide. The tensile samples were cut using scissors at the centre area of the cocoon along the major axis (i.e. the length direction of the samples is parallel to the major axis of the cocoon). The thickness of different cocoon wall samples is 393±21 μm for *B. mori*, 243±31 μm for *S. cynthia*, 277±29 μm for *A. assamensis*, and 387±31 for *A. pernyi*, respectively. The morphologies of the cocoons and the fracture surfaces from failed specimens were investigated by a scanning electron microscopy (SEM) (Supra 55VP). The silk fibre cross-section was measured from the SEM images of 50 fibres and determined from the histogram graphs of size distribution. The 180 degree peel test, which is modified from the ASTM standard test D 1876-08 used for peel resistance of adhesives [19], was performed on a Lloyd LR30K tester with a 100 N load cell. The detailed experimental and data analysis methods can be found in ref. [14]

2.2.2. Scanning Probe Microscopy (SPM)

SPM analysis was conducted on a Bruker MultiMode-8 tester in contact mode using silicon tip on cantilevers with a nominal force constant 40 N/m. Single degummed silk fibre was fixed on a metal substrate with double sided tape. The surface roughness was quantified by measuring the average roughness, R_a, which represents the arithmetic average of the deviations from the centre plane. The surface roughness calculations were based on the 1.2 μm × 1.2 μm height image after applying a 3rd order flattening routine using the V 1.40 NanoScope software.

2.3 Physicochemical Properties of Silk Fibres- Inverse Gas Chromatography (IGC)

Surface energy and specific surface area were analyzed using the IGC-Surface Energy Analyzer (Surface Measurement Systems, Alperton, Middlesex, UK). Approximately 1.5 g of each degummed silk fibre sample, cut at 5 cm lengths, was packed into individual 300 mm long by 4 mm inner diameter silanized glass columns (Surface measurement Systems, Alperton, Middlesex, UK).

In IGC, the adsorbent under investigation is placed into a column while a known adsorptive is used in the gas phase. As in analytical gas chromatography, the retention time is obtained as the fundamental parameter measured. The retention time can be converted into a retention volume, which is directly related to several physico-chemical properties of the solid (absorbent). Surface energetic heterogeneity profile can be represented by an energy distribution with surface coverage, which can provide more comprehensive understanding on the nature and population of different surface sites. IGC experiments with finite concentrations were conducted in pulse mode, by injecting a desired amount of probe molecule into the column via inert helium carrier gas. A series of n-alkanes (n-heptane, n-octane and n-nonane) and polar probes (chloroform, ethyl acetate, acetone, acetonitrile and 1, 4-dioxane) were injected at a specific fractional surface coverage and their retention times measured for a broad range of fractional surface coverage. The retention times were then converted into retention volumes and the dispersive surface energy (γ_S^D) on a solid sample was determined in accordance with standard methodology as described by Jones. [20]

Determination of the dispersive surface energy (γ_S^D) and specific free energy of desorption (ΔG^0_{SP}), as well as the acidic and basic properties of a solid sample are well documented. [21] The net retention volume (V_N), a fundamental surface thermodynamic property of the solid-vapor interaction, can be computed from Eq. 1:

$$V_N = \frac{j}{m} \cdot F \cdot (t_R - t_0) \cdot \left(\frac{T}{273.15} \right) \quad (1)$$

where j is the James-Martin correction, m is the mass of sample in the column (g), F is the carrier gas flow rate (cm^3/min), t_R is the retention time of the probe (minutes), t_0 is the mobile phase hold-up time (minutes), and T is the column temperature (K). γ_S^D can be calculated from the V_N of a series of non-polar reference probes (for example: n-hexane, n-heptane, n-octane and n-nonane) according to a standard methodology developed by Dorris and Gray where $RT\ln(V_N)$ is plotted against the number of carbon atoms of the alkane probe. γ_S^D can then be determined from the slope of the resulting linear regression, as reported in detail elsewhere. [22]

Total surface energy (γ_S^T) was defined as the sum of the dispersive energy and the specific (γ_S^{AB}) energy contributions and the surface polarity was calculated as γ_S^{AB}/γ_S^T. On the other hand, the specific (acid-base) surface energy (γ_S^{AB}) can be obtained by first measuring the ΔG^0_{SP} for different polar probe molecules (i.e. acetonitrile, acetone, ethanol, ethyl acetate and dichloromethane) on the materials. Employing the polarisation approach, the ΔG^0_{SP} values are determined from a plot of $RT\ln(V_N)$ versus the molecular polarisabilities of the probes (P_D). The values obtained for a series of non-polar n-alkanes follow a linear relationship and ΔG^0_{SP} for each polar probe is determined relative to this reference line. [23] The acid and base numbers, K_a and K_b, and hence the acid/base ratios (K_a/K_b) were determined according to the method of Gutmann. [24]

3. Results and discussion

3.1 Mechanical Properties of Silk Cocoons

The mechanical properties of cocoon walls vary considerably with the silk cocoon type. The tensile stress strain curves of the cocoon walls are shown in Figure 1 and the tensile property is summarised in Table 1. Among all the cocoon types, the *A. pernyi* cocoon wall exhibited the highest Young's modulus, breaking stress and breaking strain. The modulus of the wild *A. pernyi* was 872 MPa, which reached more than double the value of the other three cocoon types, i.e. domestic *B. mori* and *S. cynthia*, and semi-domestic *A. assamensis*. While the other three cocoon wall types had similar breaking stress (20 to 30 MPa) and breaking strain values (16% to 21%), the *A. pernyi* achieved a breaking stress of 56 MPa and a breaking strain of 41%. The high tensile stress and strain from the *A. pernyi* cocoon wall resulted in 5 to 11 time's larger absorbed energy during the loading process.

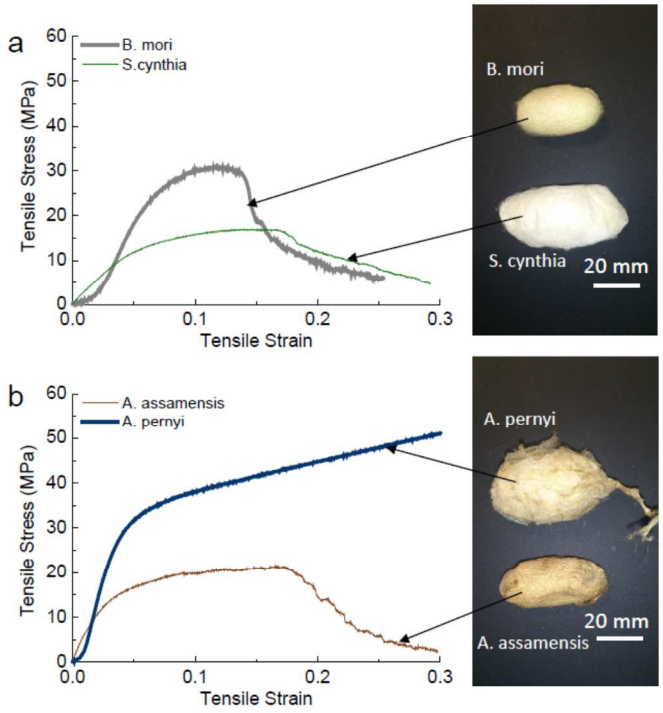

Figure 1. Tensile stress-strain curves for different types of cocoon walls

As a multilayer composite structure, the cocoon wall was tested not only along the in-plane direction but also along the interlaminar direction. Therefore, in addition to the tensile properties, the interlaminar peel resistance was also examined. The 180 degree peel tests showed that the maximum peeling load was 0.74 N and the average peeling load was 0.35 N for the *B. mori* cocoon. By comparison, the *A. pernyi* cocoon had a maximum peeling load of 4.45 N and an average peeling load of 2.51 N. The maximum work of fracture (WOF) of all tested cocoon layers was 981 J/m^2 from the *A. pernyi* outer layer, suggesting the highest interlaminar adhesion and bonding energy between the cocoon layers (Table 2). The toughness for the wild *A. pernyi* cocoon was approximately 10 times of the *B. mori* cocoon and twice the values of the *S. cynthia* and *A. assamensis* cocoon walls. The results are comparable to Chen et al.'s findings for the *B. mori* cocoon, where they observed similar nonlinear load-displacement relation with an average peeling load of 0.32 N and a WOF of 61 J/m^2 and also proved that the delamination of cocoon walls is mainly caused by the brittle fracture of the inter-layer sericin bonds. [25] As a result, the significantly higher bonding energy for the *A. pernyi* cocoon wall suggests the strongest fibroin/sericin bond in this cocoon type. The high toughness of the wild *A. pernyi* cocoon is presumably related to the higher level of protection against attack from predators and the hazardous outdoor physical environment. [14]

Table 1. Tensile properties of four types of silkworm cocoon walls

Cocoon wall type	Thickness (μm)	Nominal density (kg/m^3)	Young's modulus (MPa)	Maximum load (N)	Breaking stress (MPa)	Breaking strain (%)	Absorbed energy (J)
B. mori	393±21	377±15	365±102	49±8	30±7	16±1	0.09±0.02
S. cynthia	243±31	449±56	238±39	42±9	20±2	21±5	0.17±0.06
A.assamensis	277±29	516±28	342±72	19±1	23±6	19±7	0.05±0.009
A. pernyi	387±31	711±44	872±142	140±13	56±5	41±6	0.6±0.1

Table 2. Interlaminar peel properties of cocoon walls

Cocoon type	Wall thickness (μm)	Average peeling load (N)	Maximum peeling load (N)	Peel strength (N/m)	Work-of-fracture (J/m^2)
B. mori	393±21	0.35±0.05	0.74±0.17	62±6	119±19
S. cynthia	480±91	1.00±0.45	1.58±0.71	245±99	437±203
A. assamensis	277±29	1.21±0.56	1.43±0.40	240±89	322±121
A. pernyi	387±31	2.51±0.55	4.45±0.63	469±75	981±211

3.2 Cocoon Morphology and Tensile Fracture

As shown in Figure 2, the cocoon walls have a porous architecture with randomly distributed twin silk fibres bonded with sericin matrix. In comparison with the *B. mori* and *S. cynthia* cocoons, the silk fibres are more flat and wider in the *A. pernyi* and *A. assamensis* cocoon layers (Figure 2a-d). In general, the fibre width varies along the out-of-plane direction, i.e. the fibre width reduces towards the interior of the cocoon. Therefore the cocoon has a graded porous structure with thinner fibres and smaller pores in the inner layers. The cross-sections of the cocoon wall and silk fibres reveal the fibre packing structure and the transversal geometrical shape of the silk fibres. It appears that the *B. mori* and the *S. cynthia* cocoons have a much more porous structure than the densely packed *A. pernyi* and *A. assamensis* cocoon walls. In particular, for the *A. pernyi* cocoon, the near-rectangular silk fibres are packed in parallel to the surface and form a compact brick-like fibre assembly. The *B. mori* silk

fibres have a near-triangular-shaped cross-section and the *S. cynthia* silk fibres have more irregular fibre profiles.

After tensile failure, among all the cocoon walls, only the *A. pernyi* showed a failed planar structure, all the other types turned completely fibrous due to the weaker bond in the 3D cocoon fibrous assembly (Figure 3). It can be seen in the pulled *B. mori* silk fibres that the sericin shell detached from the fibroin core, indicating a weak bond between the fibroin and sericin. The fracture morphology shows the separation of the fibroin and sericin took place by the relative sliding of both surfaces. The *S. cynthia* silk exhibited a fibre split failure; the *A. assamensis* and the *A. pernyi* showed the ductile sericin matrix nature, which is in agreement with the reduced elastic modulus of these silk fibres as compared with *B. mori* (because of the large volume fraction of matrix which does not contribute to the fibre stiffness). Finally, the large elongation of wild silk fibres correlates well with the non-linear behaviour of composites prior to failure[26, 27]. In all the three types of silk fibres other than *B. mori*, the sericin and the fibroin are not distinguishable in the other silk types.

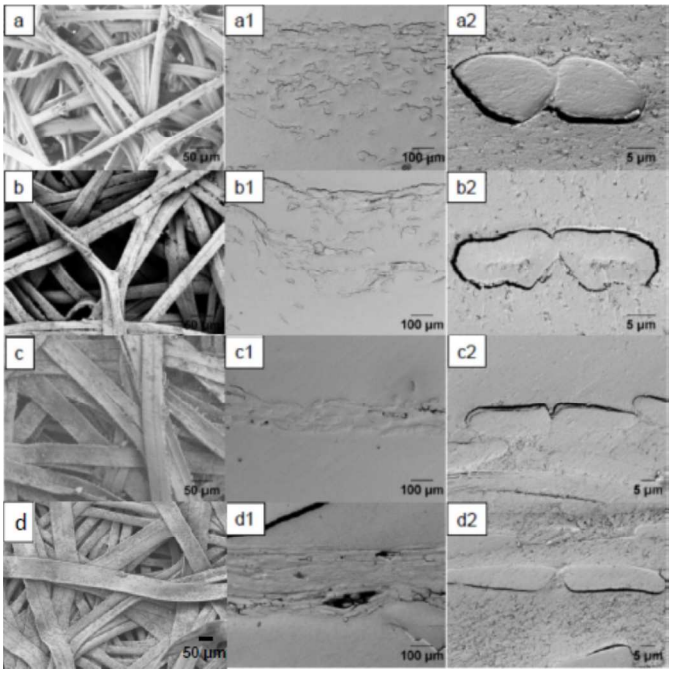

Figure 2. The outer layer, cross-section of different cocoon walls and the twin silk fibres from each type. (a), (a1) and (a2): *B. mori*; (b), (b1) and (b2): *S. cynthia*; (c), (c1) and (c2): *A. assamensis*; (d), (d1) and (d2): *A. pernyi*.

3.3 Mechanical Property and Surface Topography of Degummed Silk Fibres

Figure 4 shows the tensile stress-strain curves of the degummed silk fibres. The stress-strain curves of the *S. cynthia*, *A. assamensis* and *A. pernyi* silk fibres have a distinct yield point followed by obvious strain hardening, which is similar to the spider major ampullate silks [5]. In contrast, the *B. mori* silk lacks such distinct yield points and has much lower extensibility. It is interesting to see that the *B. mori* silk fibroin is almost as strong as the wild silk fibres despite the fact that the *A. pernyi* fibroin has a much higher breaking strain of 50% (Table 3). The *A. pernyi* fibres are 30% tougher than the domestic *B. mori* fibres and 100% tougher than the *S. cynthia* fibres. The mechanical properties of composite structure are generally determined by the fibre reinforcement properties, the fibre/matrix adhesion and the matrix properties. For the case of biological cocoon structure, the higher mechanical properties from the wild *A. pernyi* type are not only affected by the fibroin and sericin properties, but also dependent on the interfacial adhesion between the fibroin and sericin. The surface topography and roughness, and the surface energy of silk fibroin were consequently further investigated.

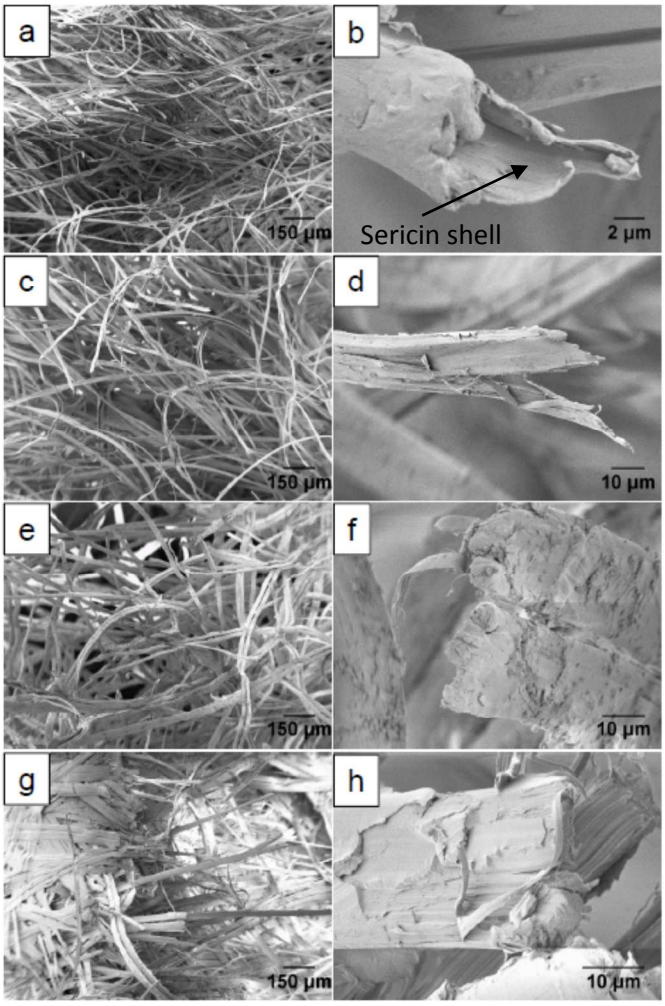

Figure 3. Tensile fracture of cocoon walls and enlarged view of broken silk fibres. (a) and (b) are *B. mori*; (c) and (d) are *S. cynthia*; (e) and (f) are *A. assamensis*; (g) and (h) are *A. pernyi*.

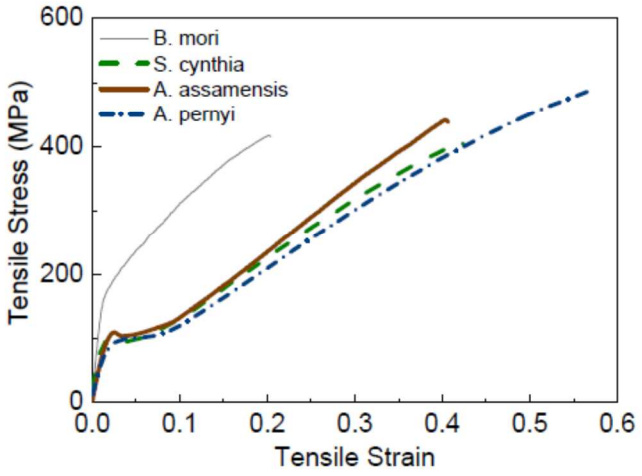

Figure 4. Tensile stress-strain curves for degummed single silk fibres

Table 3. Tensile properties of the degummed single silk fibres

Silk type	Single fibre cross-section area (μm^2)	Young's modulus (GPa)	Maximum load (cN)	Maximum stress (MPa)	Strain at maximum stress (%)	Toughness (J/m^3)
B. mori	74±2	13.3±1.8	4.7±0.81	635±108	22±5	1.0×10^8
S. cynthia	196±26	4.43±0.60	5.6±1.7	284±88	34±13	6.1×10^7
. assamensis	231±22	5.70±0.47	11.4±1.1	495±48	51±6	1.4×10^8
A. pernyi	350±37	4.98±0.56	14.9±1.9	426±55	51±7	1.3×10^8

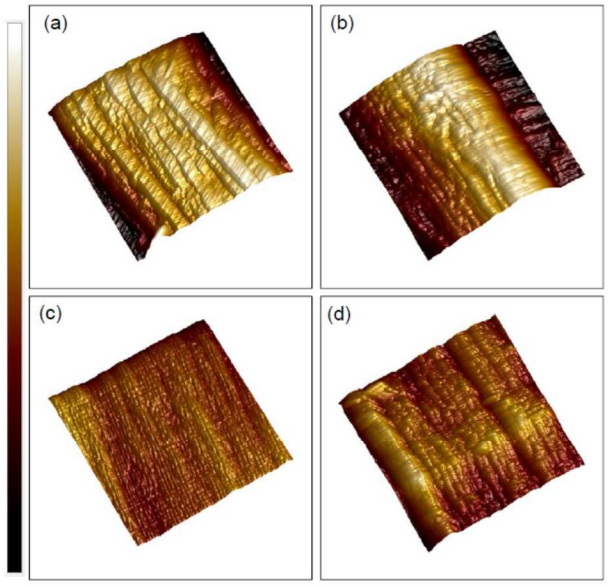

Figure 5. SPM topography of degummed silk fibre surfaces. a) *B. mori*; b) *S. cynthia*; c) *A. assamensis*; d) *A. pernyi*. The z-color bar on the left ranges from -65 to 65 nm.

3.4 Silk Fibre Surface Topography

The SPM images show the presence of distinct longitudinal ridges and striations along the fibre axis of the four silk fibre types (Figure 5). The *A. assamensis* surface shows finer and lower grooves than the other three types. Surface roughness analysis was based on the SPM height images taken over a 1.2 µm by 1.2 µm area. The effect of fibre curvature needs to be removed before the surface roughness can be measured. In the current work this was done by applying a 3rd order flattening routine. The average roughness is 5.00 nm for *B. mori*, 7.29 nm for *S. cynthia*, 3.54 nm for *A. assamensis* and 6.76 nm for *A. pernyi*. The roughness value was the lowest for the *A. assamensis* which has the finest surface texture and the highest for the *S. cynthia* which was more than twice the value of the *A. assamensis*.

Increasing surface roughness of biomaterials has shown advantageous effects on the cell attachment for healing and bone formation [3]. Silk fibroin is a native protein from silkworm fibre and is a remarkably stable and mechanically robust protein biomaterial, as evidenced by the ability to be autoclaved for sterilization and is amendable to ethylene oxide sterilization and gamma irradiation [28]. It can be conveniently employed in tissue engineering systems, drug release systems, bio-optics and bioelectronics applications. [1, 29] The combination of excellent mechanical and surface properties of the wild *A. pernyi* silk fibroin may pave the way for its broader use for biomedical applications.

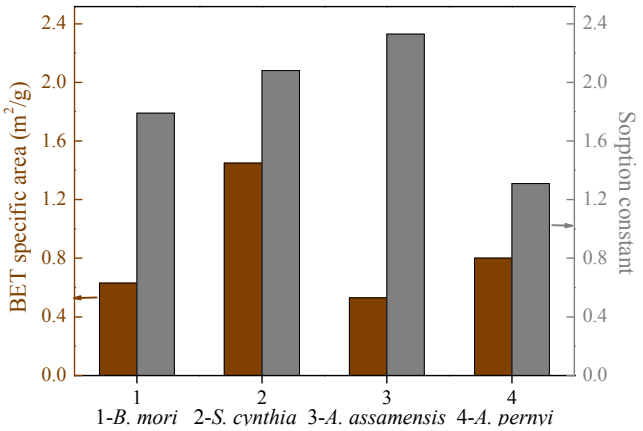

Figure 6. Specific surface area determined from Octane sorption isotherm

3.5 Surface Energy

IGC can accurately determine the adsorption isotherms at ambient temperatures and atmosphere pressure using organic probe molecules. It allows the Brunauer, Emmett and Teller (BET) surface area to be measured, especially for the materials with low surface area. The sorption constant is related to the affinity of the solid with the adsorbate and the heat of adsorption. The BET surface area and the sorption constant for four types of silk fibroin are shown in Figure 6. The *S. cynthia,* which has the highest surface roughness value, also has the highest BET surface area. In fact, the BET surface area results for silk fibroin follow the same sequence of the fibre surface roughness measurement. However, since the fineness of fibres is not the same for different silk fibre types and some silk fibres have pores, the BET surface area was affected by these factors as well. It is generally known that the higher the value of sorption constant, the higher the interaction [30]. Hence the surfaces of the *A. assamensis*, *S. cynthia* and *B. mori* silk fibroin may facilitate with better interaction with the absorbate.

Using IGC at finite concentration conditions generates surface energy (total, dispersive, specific or polar) as a function of surface

coverage. Surface heterogeneity of silk fibres has not been sufficiently studied in silk fibres, despite its importance in many applications. There are two types of surface heterogeneity: structural and energetic. The former refers to the distribution of pore size and shape, being mainly a geometrical effect determined by the correlation between probe molecule size and pore diameter, whereas the latter refers to the distribution of surface sites of distinct energetic levels including surface groups, impurities and/or surface irregularities.[30] A completely flat line is indicative of an energetically homogeneous surface. The total surface energy traces (γ_S^T) for four types of silk fibres are shown in Figure 7. All samples are energetically heterogeneous since the surface energy changes as a function of surface coverage. The total surface energy of the *A. pernyi* fibres varies from a minimum average value of 44 mJ/m^2 to a maximum value of 52 mJ/m^2 and the total surface energy of the *B. mori* fibres varies from a minimum average value of 43 mJ/m^2 to a maximum value of 52 mJ/m^2. The range of the total surface energy for the *S. cynthia* is from 41 mJ/m^2 to 47 mJ/m^2 and that for the *A. assamensis* is from 45 mJ/m^2 to 52 mJ/m^2.

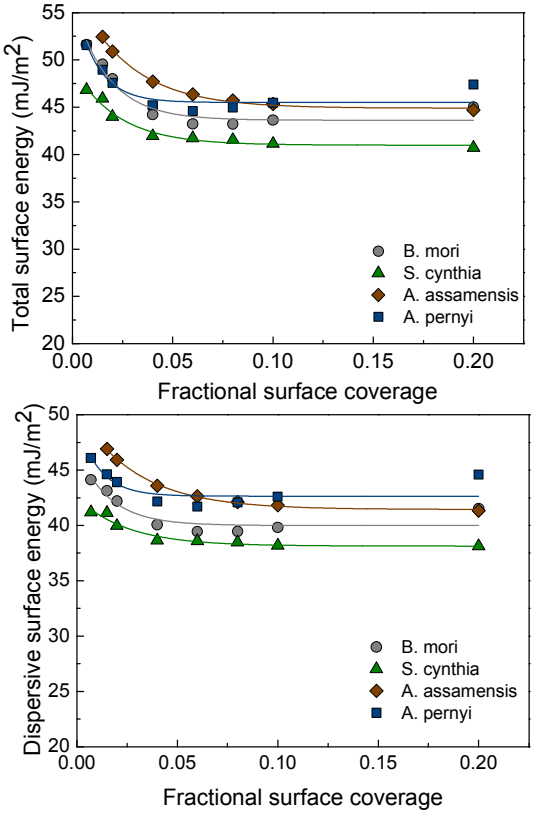

Figure 7. Total surface energy (γ_S^T) and dispersive surface energy (γ_S^D) for the degummed *B. mori*, *S. cynthia*, *A. assamensis* and *A. pernyi* silk fibres.

The total surface energy (γ_S^T) is made up of the dispersive (non-polar) interactions (γ_S^D) and the specific (acid–base or polar) contributions (γ_S^{AB}). The dispersive component arises from London, van der Waals and Lifshitz forces[31] and the acid–base component arises from Lewis acid–base interactions and hydrogen bonds. [24] It can be seen from Figures 7 and 8 that all the silk fibres are heterogeneous in both dispersive and acid-base surface energies. Dispersive surface energy (γ_S^D) profiles in Figure 7 show that all silk fibres are energetically active and heterogeneous. The dispersive surface energy for the four silk samples changes as a function of surface coverage (up to 20% of surface coverage). The *A. pernyi* and the *A. assamensis* silk fibres have higher γ_S^D than the other two types. The *A. assamensis* silk fibres, in particular, also possess wider γ_S^D distribution, ranging from 41 to 47 mJ/m^2 compared to the *B. mori* (40-44 mJ/m^2), *S. cynthia* (38-41 mJ/m^2) and *A. pernyi* silk fibres (42-46 mJ/m^2). Similar dispersive surface energy values for jute, silk floss, coir and sisal (41.9, 39.5, 39.1 and 38.4 mJ/m^2, respectively) have been reported. [32] The higher γ_S^D of the *A. pernyi* and the *A. assamensis* silk fibres may be indicative of different surface groups with higher γ_S^D. The wider γ_S^D variation of the *A. assamensis* silk fibres indicates their surfaces contain more different levels of energetic sites. [33] The higher γ_S^D can also be an indication of more hydrophobic active sites. On the other hand, the polar surface energy profiles in Figure 8 show energetically heterogeneous nature for all types of silks. In particular, the distribution of polar surface energy of the *B. mori* silk fibres varies from 3.5 to 7.5 mJ/m^2, which is higher than other types. This may be due to the presence of more polar surface groups on the *B. mori* silks. However, all silk fibres were degummed by using the soap-soda method. During the degumming process, sericin is hydrolyzed and solubilized and at least one type of non-covalent interaction such as hydrogen bonds was weakened. Therefore the polar surface energy would be affected by degumming as the result that the acid–base component of the total surface energy arises from Lewis acid–base interactions and hydrogen bonds.

The surface chemistry of the samples was assessed using the Gutmann acid (K_a) and base (K_b) numbers, determined based on the Gutmann approach. Values of the samples were calculated using the Gibs free energy values of polar probes at that particular surface coverage. It is clearly seen from Figure 8 that the base numbers (K_b) are consistently higher than the acid numbers (K_a) ($K_a/K_b < 1$), indicating that the surfaces are generally more basic in nature [34], which may be attributed to higher concentration of electron-donating surface functional groups. Figure 8 shows that the acid base ratios are higher for the *B. mori* and the *A. assamensis* silks which indicates that these silk samples possess marginally higher concentrations of electron-accepting surface functional groups. The work by Fowkes [35, 36] has indicated that the acid-base interactions, in which one phase acts as an electron donor (base) and the other acts as an electron acceptor (acid), play a significant role in interfacial adhesion. As a result, surface modification of the fibres and/or the matrix of composites must be performed to modify the acid-base interactions at the matrix–fibre interface in order to improve the mechanical performance of the composites constituted by these fibres.

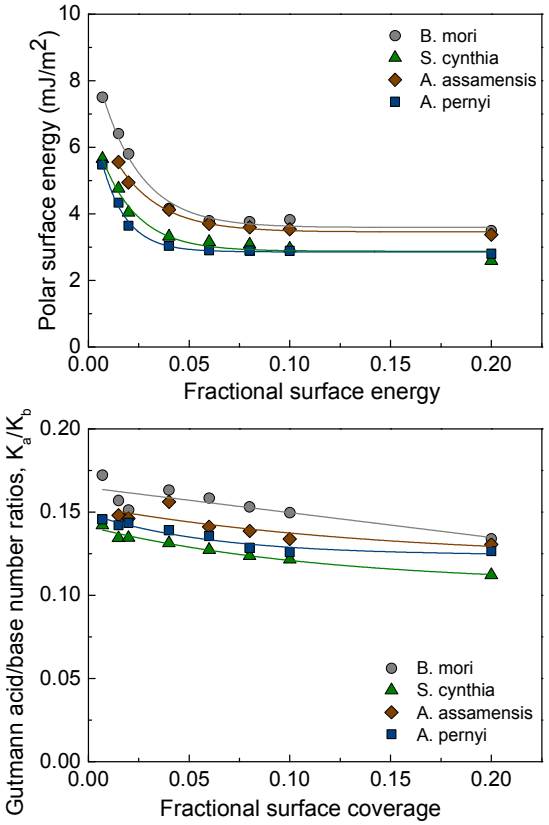

Figure 8. Polar surface energy (γ_S^{AB}), Gutmann acid (K_a) and base (K_b) number ratios for the degummed *B. mori*, *S. cynthia*, *A. assamensis* and *A. pernyi* silk fibres.

4. Conclusions

Four types of silk cocoons including the domesticated (*B. mori* and *S. cynthia*), semi-domesticated (*A. assamensis*) and wild type (*A. pernyi*) were investigated in this work. Among all cocoon types, the *A. pernyi* cocoon wall exhibited the highest Young's modulus, breaking stress and breaking strain, which also resulted in 5 to 11 time's larger absorbed energy during the loading process over other cocoon types. After tensile failure, among all the cocoon walls, only the *A. pernyi* showed a failed planar structure, all the other types turned completely fibrous due to the less strong bond in the 3D cocoon fibrous assembly. The morphology of the cocoon structures reveals that the *A. pernyi* cocoons have near-rectangular silk fibres packed in parallel to the surface and form a compact brick-like fibre assembly. However, the *B. mori* and the *S. cynthia* cocoons have much more porous structure with silk fibres having either near-triangular-shaped cross-section or irregular fibre profiles. The higher mechanical properties from the wild *A. pernyi* cocoon are not only affected by the fibroin and sericin properties, but also dependent on the interfacial adhesion between the fibroin and sericin. The fibroin surface roughness is higher for the *S. cynthia (*7.29 nm) and the *A. pernyi* (6.76 nm) cocoon types. The combination of excellent mechanical and more heterogeneous surface properties of the wild *A. pernyi* silk fibroin may pave the way for its broader use for biomedical applications. The surface energetics of materials are known to have important implications in processes involving interfacial interactions, as in wetting, coating, cohesion/adhesion etc. All silk fibroin samples are energetically heterogeneous, i.e. the surface energy changes as a function of surface coverage. The *A. pernyi* fibroin has higher dispersive surface energy and the *A. assamensis* fibroin has wider dispersive energy variation, suggesting their surfaces contain more different levels of energetic sites. The Gutmann acid/base values indicate that the silk fibroin surfaces are generally more basic in nature, which may be attributed to higher concentration of electron-donating surface functional groups.

Acknowledgements

The authors would like to acknowledge the funding support from the Australian Research Council (ARC) through a Discovery project DP 120100139. Dr. Anett Kondor's assistance for the IGC data analysis is appreciated.

Notes and references

[a] Australian Future Fibres Research and Innovation Centre, Institute for Frontier Materials, Deakin University, VIC 3217, Australia.
[b] Biophysics and Micro/Nanostructures Lab, Department of Physics, Faculty of Science, National University of Singapore, 117542, Singapore.
[c] School of Textile Science and Engineering, Wuhan Textile University, Wuhan 430073, China.

Electronic Supplementary Information (ESI) available: [details of any supplementary information available should be included here]. See DOI: 10.1039/b000000x/

1. F. G. Omenetto and D. L. Kaplan, *Science*, 2010, **329**, 528-531.
2. H.-P. Zhao, X.-Q. Feng, W.-Z. Cui and F.-Z. Zou, *Eng Fract Mech*, 2007, **74**, 1953-1962.
3. C. Vepari and D. L. Kaplan, *Prog Polym Sci*, 2007, **32**, 991-1007.
4. Q. Fang, D. Chen, Z. Yang and M. Li, *Mater Sci Eng C*, 2009, **29**, 1527-1534.
5. N. Du, Z. Yang, X. Y. Liu, Y. Li and H. Y. Xu, *Adv Funct Mater*, 2011, **21**, 772-778.
6. N. Du, X. Y. Liu, J. Narayanan, L. Li, M. L. M. Lim and D. Li, *Biophys J*, 2006, **91**, 4528-4535.
7. Y. Liu, Z. Shao and F. Vollrath, *Nat Mater*, 2005, **4**, 901-905.
8. J. Zhang, R. Rajkhowa, J. Li, X. Y. Liu and X. Wang, *Mater Des*, 2013, **49**, 842-849.
9. F. Chen, D. Porter and F. Vollrath, *Mater Sci Eng C*, 2012, **32**, 772-778.
10. C. Fu, D. Porter, X. Chen, F. Vollrath and Z. Shao, *Adv Funct Mater*, 2011, **21**, 729-737.
11. L. P. Lounibos, *Anim Behav* 1975, **23**, 843-853.
12. T. Kaise, M. Miura, H. Morikawa and W. Iwasa, *J Insect Biotechnol Sericology*, 2003, **72**, 171-175.
13. A. Kafi, M. Huson, C. Creighton, J. Khoo, L. Mazzola, T. Gengenbach, F. Jones and B. Fox, *Compos Sci Technol*, 2014, **94**, 89-95.
14. J. Zhang, J. Kaur, R. Rajkhowa, J. Li, X. Liu and X. Wang, *Mater Sci Eng C*, 2013, **33**, 3206-3213.
15. J. Zhang, J. Kaur, R. Rajkhowa, J. Li, X. Liu and X. Wang, presented in part at the the 8th International Conference on Structure Integrity and Fracture, Melbourne, 2013.
16. Y.-Q. Zhao, H.-Y. Cheung, K.-T. Lau, C.-L. Xu, D.-D. Zhao and H.-L. Li, *Polym Degrad Stabil*, 2010, **95**, 1978-1987.

17. H.-Y. Cheung, K.-T. Lau, Y.-F. Pow, Y.-Q. Zhao and D. Hui, *Composites Part B*, 2010, **41**, 223-228.
18. B. Bax and J. Müssig, *Compos Sci Technol*, 2008, **68**, 1601-1607.
19. D. Plackett, T. Løgstrup Andersen, W. Batsberg Pedersen and L. Nielsen, *Compos Sci Technol*, 2003, **63**, 1287-1296.
20. M. D. Jones, P. Young and D. Traini, *Adv Drug Deliv Rev*, 2012, **64**, 285-293.
21. F. Thielmann, *J Chromatogr A*, 2004, **1037**, 115-123.
22. G. M. Dorris and D. G. Gray, *J Colloid Interf Sci*, 1980, **77**, 353-362.
23. J. B. Donnet, S. J. Park and H. Balard, *Chromatographia*, 1991, **31**, 434-440.
24. V. Gutmann, *The donor–acceptor approach to molecular interactions*, Plenum Press, New York, 1978.
25. F. Chen, D. Porter and F. Vollrath, *Acta Biomater*, 2012, **8**, 2620-2627.
26. P. Poza, J. Pérez-Rigueiro, M. Elices and J. Llorca, *Eng Fract Mech*, 2002, **69**, 1035-1048.
27. G. Nadiger and V. Halliyal, *Colourage*, 1984, **31**, 23-32.
28. X. Hu, S.-H. Park, E. S. Gil, X.-X. Xia, A. S. Weiss and D. L. Kaplan, *Biomaterials*, 2011, **32**, 8979-8989.
29. Y. Wang, H. J. Kim, G. Vunjak-Novakovic and D. L. Kaplan, *Biomaterials*, 2006, **27**, 6064-6082.
30. N. Cordeiro, C. Gouveia, A. G. O. Moraes and S. C. Amico, *Carbohyd Polym*, 2011, **84**, 110-117.
31. F. M. Fowkes, *Ind Eng Chem*, 1964, **56**, 40-52.
32. R. H. Mills, D. J. Gardner and R. Wimmer, *J Appl Polym Sci*, 2008, **110**, 3880-3888.
33. P. P. Ylä-Mäihäniemi, J. Y. Y. Heng, F. Thielmann and D. R. Williams, *Langmuir*, 2008, **24**, 9551-9557.
34. J. Y. Y. Heng, D. F. Pearse, F. Thielmann, T. Lampke and A. Bismarck, *Compos Interface*, 2007, **14**, 581-604.
35. F. M. Fowkes, *Rubber Chem Technol*, 1984, **57**, 328-343.
36. F. M. Fowkes and M. A. Mostafa, *Ind Eng Chem Prod Rd*, 1978, **17**, 3-7.

